JOURNAL OF GEOPHYSICAL RESEARCH: SOLID EARTH, VOL. 118, 1795–1806, doi:10.1002/jgrb.50104, 2013

The use of GPS horizontals for loading studies, with applications to northern California and southeast Greenland

John Wahr,[1] Shfaqat A. Khan,[2] Tonie van Dam,[3] Lin Liu,[4] Jan H. van Angelen,[5] Michiel R. van den Broeke,[5] and Charles M. Meertens[6]

Received 23 August 2012; revised 15 January 2013; accepted 20 January 2013; published 25 April 2013.

[1] We describe how GPS measurements of horizontal crustal motion can be used to augment vertical crustal motion measurements, to improve and extend GPS studies of surface loading. We show that the ratio of the vertical displacement to the horizontal displacement, combined with the direction of the horizontal motion, can help determine whether nearby loading is concentrated in a small region (for example, in a single lake or glacier), and where that region is. We illustrate this method by applying it to two specific cases: an analysis of GPS data from northern California to monitor the level of Lake Shasta, and the analysis of data from a single GPS site in southeast Greenland to determine mass variability of two large, nearby outlet glaciers: Helheim Glacier and Midgaard Glacier. The California example serves largely as a proof-of-concept, where the results can be assessed by comparing with independent observations (Lake Shasta tide gauge data, in this case). Our Greenland results show that both Helheim and Midgaard have experienced notable interannual variations in mass loss rate over the last decade. Helheim's mass loss accelerated rapidly in mid-2003, decelerated in late 2005, and increased again in 2008–2009 before returning to about its pre-2003 rate in late 2010. Midgaard's mass loss accelerated in mid-2004, and remained more-or-less constant before returning to its pre-2003 rate in late 2008.

Citation: Wahr, J., S. A. Khan, T. van Dam, L. Liu, J. H. van Angelen, M. R. van den Broeke, and C. M. Meertens (2013), The use of GPS horizontals for loading studies, with applications to northern California and southeast Greenland, *J. Geophys. Res. Solid Earth, 118*, 1795–1806, doi:10.1002/jgrb.50104.

1. Introduction

[2] Global Positioning System (GPS) measurements of crustal motion have proven useful for studying surface loading [e.g., *Sauber et al*., 2000; *Heki*, 2004; *Bevis et al*., 2005; *van Dam et al*., 2007]. A change in the distribution of ice, snow, water, or atmospheric mass in a region, causes the Earth to deform. By monitoring the deformation with GPS, it is possible to place constraints on the change in mass. Although there have been exceptions [e.g., *Sauber et al*., 2000; *Sauber and Molnia*, 2004; *Grapenthin et al*., 2006], most previous loading studies have focused on the vertical component of crustal motion. Here, we describe some simple concepts that can be useful for incorporating observations of horizontal motion into studies where the loading is likely to be dominated by one or more concentrated sources. We first develop a general theoretical framework for optimally combining horizontal and vertical displacements into a single analysis. We then apply this framework to GPS data from sites in northern California and from a site in southeast Greenland, to help determine changes in mass in a nearby lake (Lake Shasta) and in nearby outlet glaciers, respectively.

[1]Department of Physics and Cooperative Institute for Research in Environmental Sciences, University of Colorado, Boulder, Colorado, USA.
[2]DTU Space-National Space Institute, Technical University of Denmark, Department of Geodesy, Kgs. Lyngby, Denmark.
[3]Research Unit Engineering Sciences, University of Luxembourg, Luxembourg City, Luxembourg.
[4]Department of Geophysics, Stanford University, Stanford, California, USA.
[5]Institute for Marine and Atmospheric Research, Utrecht University, Utrecht, The Netherlands.
[6]UNAVCO, Boulder, Colorado, USA.

Corresponding author: J. Wahr, Department of Physics and Cooperative Institute for Research in Environmental Sciences, University of Colorado, Boulder, Colorado, USA. (wahr@anquetil.colorado.edu)

2169-9313/13/10.1002/jgrb.50104

2. A Qualitative Description

[3] The placement of a load on the Earth's surface causes deformation of the underlying solid Earth and displacements of its surface. GPS measurements of those displacements can provide information about the load. If the entire loading pattern consists of just a single point mass at a known location (and the GPS measurements are noise-free), then observations of the uplift would uniquely determine the amplitude of the load. If, however, there are loads in more than one location, or if the load is spread broadly over the surface, then inversion for the mass distribution from the uplift data is non-unique. The inclusion of data from several GPS sites in the vicinity can help. But, depending on the complexity of the load's spatial pattern, the data are still not likely to yield

a unique inversion. Here, we explore how the use of horizontal displacements can improve this situation.

[4] Suppose a point mass load is placed on the Earth's surface in the vicinity of a GPS site. The deformation induced by the load will cause that site to subside and to move toward the load (see text below). Conversely, if a load is removed, the site uplifts and moves away from the load.

[5] Suppose you somehow know that there has been a mass change at one of two locations—one north of the GPS site and one south of it; but you do not know which location, and you do not know how large the mass change was. The GPS vertical results, by themselves, cannot tell you the location. If you see uplift, for example, you know there was mass loss, but you do not know where. Alternatively, suppose you see southward horizontal motion but you do not record the vertical. Then you know that either the northern location was losing mass or the southern location was gaining mass, but you cannot differentiate between these two possibilities. But suppose you use both the vertical and the horizontals, and you see both uplift and southward motion. The only possibility in that case would be mass loss from the northern location. You can then use the measured amplitude of the GPS signal—either the vertical, or the horizontal, or both—together with the known distance to that northern location to infer the total mass loss at that location.

[6] The vertical displacement from a concentrated mass load is larger than the horizontal displacement. We show below that for a localized load on a realistically stratified, spherical, elastic Earth, the ratio of the vertical displacement to the horizontal displacement is between 2.0 and 3.0, depending on how far away the load is. The ratio tends to be closer to 3.0 for a nearby load, and closer to 2.0 for a distant load. (*Pinel et al*. [2007] obtained similar ratios for an elastic half space.)

[7] Suppose, though, that there are loads at more than one location. For example, suppose there is mass loss at both the northern and southern locations mentioned above. Both those loads will cause uplift. But the removal of the northern load will cause southward motion, and the removal of the southern load will cause northern motion. Thus, the two uplift signals will add constructively, but the two horizontal signals will tend to cancel. In that case, the ratio of vertical to horizontal will likely be larger than 2.0–3.0. Alternatively, suppose there is a mass loss at the northern location, but a mass gain at the southern location. Then the northern mass will cause uplift but the southern mass will cause subsidence, and so there will be cancelation in the vertical. But both loads will cause southward motion, and so the horizontal displacements will add constructively. In this case, the ratio of vertical to horizontal will likely be smaller than 2.0–3.0. We note that this latter case is somewhat unlikely, since usually most concentrated loads (e.g., lakes or glaciers) in a region are apt to be increasing or decreasing together.

3. Theory

[8] Suppose we place a uniform disc of mass with angular radius α, on the surface of a spherical, self-gravitating, elastic Earth. We describe the mass in terms of the equivalent thickness of water, h. The total mass of the disc is $M = h\ \rho_w 2\pi\ (1 - \cos\alpha)\ a^2$, where ρ_w is the density of water and a is the Earth's radius. The mass per area as a function of the angular distance, θ, away from the center of the mass load, is [*Farrell*, 1972; p. 773]:

$$\gamma(\theta) \;=\; \sum_{n=0}^{\infty} \Gamma_n P_n(\cos\theta) \tag{1}$$

where the P_n are Legendre polynomials, and

$$\begin{aligned} \Gamma_n &= \frac{1}{2}\left[P_{n-1}(\cos\alpha) \;-\; P_{n+1}(\cos\alpha)\right] \qquad \text{for } n > 0 \\ \Gamma_0 &= \frac{1}{2}\ (1 - \cos\alpha) \end{aligned} \tag{2}$$

[9] The perturbation in the gravitational potential at the Earth's surface is [*Farrell*, 1972; equation (31)]:

$$\Phi(\theta) \;=\; \sum_{n=0}^{\infty} \Gamma_n \frac{4\pi G a}{2n+1} P_n(\cos\theta) \tag{3}$$

where G is Newton's gravitational constant. The displacements of the Earth's surface in the vertical (positive = up) and horizontal (positive = away from the load) directions caused by this gravitational potential are, respectively [*Farrell*, 1972; equations (28) and (32)]:

$$s_{\text{up}} = \sum_{n=0}^{\infty} h_n \Gamma_n \frac{4\pi G a}{g(2n+1)} P_n(\cos\theta) \tag{4}$$

$$s_{\text{away}} = \sum_{n=0}^{\infty} l_n \Gamma_n \frac{4\pi G a}{g(2n+1)} \frac{dP_n(\cos\theta)}{d\ \theta} \tag{5}$$

where h_n and l_n are load Love numbers and g is the gravitational acceleration at the Earth's surface. We compute those load Love numbers up to degree 2300 using the numerical methods employed by *Dahlen* [1976], supplemented by the $n = \infty$ limit computed as described by *Farrell* [1972], for Earth model PREM with a continental crust [*Dziewonski and Anderson*, 1981].

[10] Suppose a uniform disc of mass, with radius 20 km and with mass-per-area equivalent to that of 1 m of water thickness, is removed from the Earth's surface. The Earth then deforms so that any nearby point on the Earth's surface moves upward and away from the center of the disc. Figure 1a shows both the vertical (positive is uplift) and the horizontal (positive is away from the disc center) displacements, as a function of the distance to the disc's center. The vertical line marks the boundary of the disc. Note that the uplift (orange curve) is maximum at the center and decreases rapidly with increasing distance until about two disc radii from the center, after which there is a slowdown in the rate of decrease with increasing distance, resulting in a long non-zero tail.

[11] The horizontal displacement (the blue curve in Figure 1a) is zero at the disc center. That is because a point at the center sees as much of the disc on one side as on the other, so there is no preferred direction of motion. As we consider points still inside the disc radius but at increasing distance from the center, more of the disc starts to lie on one side of the point than on the other, and so the net horizontal displacement increases. Once we move outside the disc, the disc is all on the same side of the point, and is moving farther away (with increasing distance), so the horizontal displacement starts to decrease.

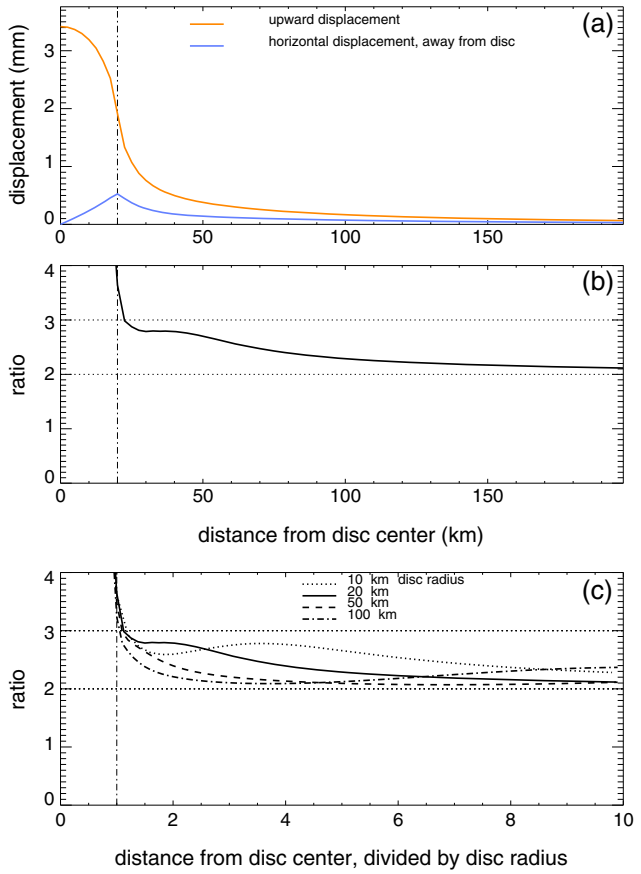

Figure 1. (a) the vertical (positive upward) and horizontal (positive away from the disc center) crustal displacements caused by removing a uniform disc load of radius 20 km and 1 m equivalent water thickness. Results are given as a function of the distance to the center of the disc. The vertical dot-dashed line marks the edge of the disc. Results are computed for Earth model PREM [*Dziewonski and Anderson*, 1981]. (b) The ratio of the vertical to horizontal displacements shown in (a). (c) Similar to Figure 1b, but for discs of various radii. In Figure 1c, the distances shown on the x axis have been normalized by dividing by the radius of the disc.

[12] The horizontals, though, do not decrease with distance quite as quickly as the verticals do. Think of the disc mass as consisting of lots of little masses spread over the disc area. Removing the disc mass is equivalent to simultaneously removing each of those little masses. The removal of any one of those little masses causes the observation point to uplift and to move away from the location of that mass. All the contributions to the uplift simply add together, to produce the total uplift from the disc. But the horizontal displacements from the different masses are in somewhat different directions, and so there is some cancelation: the amplitude of the combined horizontal displacement is smaller than the sum of the individual amplitudes. Basically, the verticals from the little masses add as scalars, whereas the horizontals add as vectors. The cancelation decreases as the observation point moves farther away from the disc, since then the observation point begins to see all the little masses as lying more nearly in the same direction. Thus, at points far distant from the load, the horizontal displacements caused by each little mass tend effectively to add as scalars, just like the uplift values. And so the ratio of the net uplift to the net horizontal displacement is smaller at points far distant from the load than it is at nearby points.

[13] Figure 1b shows the ratio of the vertical amplitude to the horizontal amplitude, caused by this disc load. The dashed horizontal lines are positioned at values of 2.0 and 3.0. Note that the ratio falls off with distance, which is a consequence of the fact that the horizontals are proportionally smaller than the verticals just outside the disc. Once the distance from the disc's edge is roughly 10% of the disc's radius, the ratio has fallen to 3.0 and decreases down to about 2.1 at a distance of 10 disc radii—i.e., a distance where the displacement amplitudes from this single disc are typically small enough that it could be difficult to pick out the signal in a GPS record. The values of this ratio seem to be relatively insensitive to Earth structure. For example, when *Farrell's* [1972] results for the much older and less well-constrained Gutenberg-Bullen A structural model are used, the ratios are smaller than those given here for PREM, but only by 5–10%.

[14] In the examples below, we use this range of 2.0–3.0 as a guide to determining whether a GPS signal is caused by a single isolated load or not. To get a sense of how this ratio might depend on the extent of the load, Figure 1c shows results for this ratio for uniform discs of various radii. In each case, the distance on the x axis has been scaled by dividing by the disc's radius. And in each case, the ratio drops to 3.0 when the distance outside the disc has increased to about 10% of the disc radius. The ratio stays above 2.0 as the distance continues to increase.

[15] Surface loading in the vicinity of a GPS site can be concentrated into well-defined regions, such as glaciers or lakes. Or, it can be spread over broad regions, such as the loading from large-scale soil moisture variability or atmospheric pressure variations. Applications of the concepts described above are likely to be most useful in situations where there are significant contributions from concentrated loads. In the following sections, we consider examples of two such cases.

4. Application to Lake Shasta in Northern California

[16] In this section we consider four continuous Plate Boundary Observatory GPS sites (P349, P341, P060, and P338) located near Lake Shasta, a manmade reservoir in northern California (Figure 2b). P349 is ~2 km due south of the lake. The other three sites are farther (P341 and P060 are ~20 km from the lake, and P338 is ~40 km from it). These four sites were established in September to October 2005. The lake area is about 120 km^2, which is the area of a disc of radius 6 km. The lake level is monitored with tide gauges. Lake level observations between 1990 and 2012 (Figure 3) show significant seasonal variability, superimposed on a dramatic ~15 m lake level decrease in 2007 with a recovery in 2010. This 2007–2010 feature coincides with the timing of a severe drought in California, when precipitation was 25% below the long term average and river stream flow was 40% below average [*Christian-Smith et al.*, 2011]. The onset and recovery from the drought overlap the time span of the GPS observations. Here, we examine how the GPS crustal motion measurements can be used to independently determine this drought-related feature in the lake level.

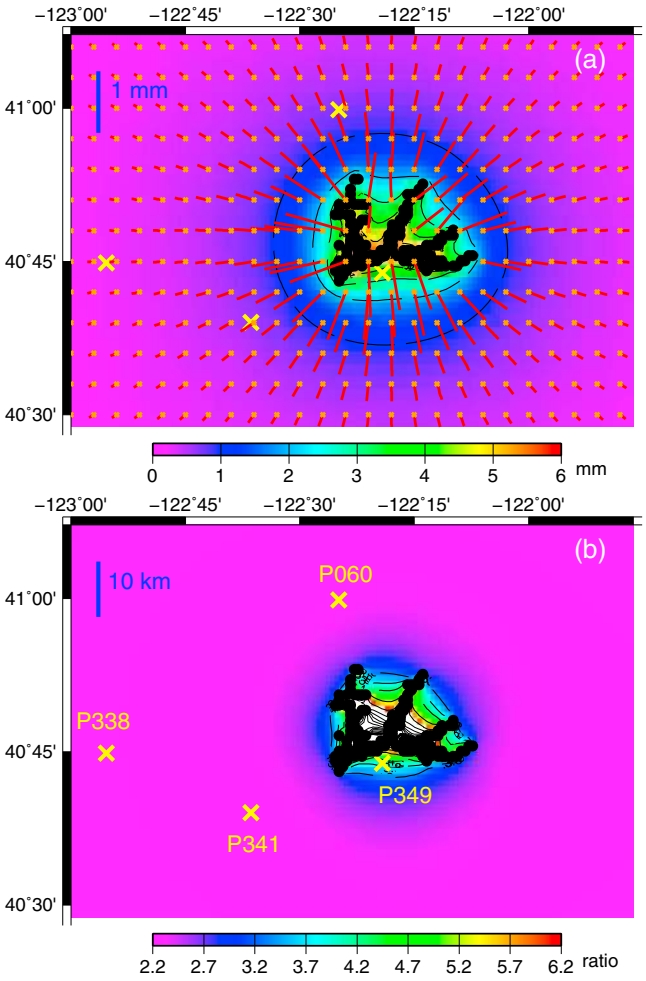

Figure 2. (a) The expected vertical (positive upward) and horizontal displacements, caused by a uniform 10 m decrease in the level of Lake Shasta. The uplift displacements are indicated by the color contours. The horizontal displacements are shown by the red lines: the length of a line represents the amplitude (the length of the vertical blue line in the upper left corresponds to 1 mm of horizontal displacement), and the direction of the line as it moves away from its yellow dot represents the direction of motion. Lake Shasta is in black. The four GPS sites are shown by the yellow x's. (b) The ratios of the vertical to horizontal amplitudes shown in Figure 2a. The names of the GPS sites are indicated. The length of the vertical blue bar corresponds to 10 km of geographic distance. The white region around the lake corresponds to values of the ratio that are larger than the maximum 6.2 value given in the color scale.

[17] We use the loading displacement Green's functions for Earth model PREM (with a continental crust), as tabulated by *Jentzsch* [1997], to model the crustal motion signals that would be produced by a uniform change in the level of Lake Shasta. Figure 2a shows the vertical and horizontal displacements that would be caused by a 10 m fall in lake level. As expected, the displacements are largest closest to the lake, and the direction of horizontal motion is away from the lake. Figure 2b shows the predicted vertical-to-horizontal ratio. The ratio is fairly uniform, at about 2.3, over most of the region. But at P349 (the site closest to, and just south

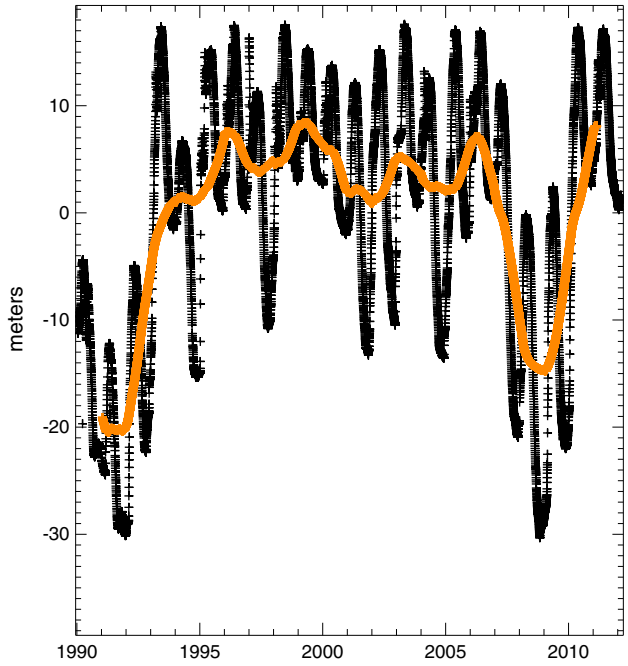

Figure 3. The black plus signs are daily Lake Shasta lake level values, as determined by tide gauge data available from the California Department of Resources (http://cdec.water.ca.gov/cgi-progs/queryDaily?SHA). An arbitrary lake level mean has been removed. The orange line is a smoothed version of the daily values. The dramatic dip between 2007 and 2010 coincides with a period of drought in northern California.

of the lake), the ratio rises to about 4.0. This is because to a GPS receiver at that location the lake appears to be spread over a wide range of azimuths. In that situation, the vertical contributions from every small bit of lake area add constructively, whereas the horizontal contributions tend to partially cancel one another. We apply the Figure 2 numerical results to the GPS data to reproduce the drought-related lake feature, as follows.

[18] The top row of Figure 4 shows daily values for the upward, eastward, and northward coordinates determined by GPS data at P349, between 28 October 2005 and 22 October 2011, as produced by the Plate Boundary Observatory Analysis Centers (PBOACs). Data from 1112 PBO GPS stations, as well as from another approximately 100 auxiliary stations in and around North America, are processed on a daily basis by the PBOACs. The auxiliary stations include reference stations in the International GNSS Service (IGS) network that provide ties to the IGS realization of the International Terrestrial Reference Frame (ITRF2008). Data are processed independently by the PBAOCs using either GIPSY point positioning with network bias fixing or GAMIT network double difference solutions. Results using these two independent GPS analysis packages are combined to form the final estimated position time series products. The estimated position time series are rotated, translated, and scaled to ITRF2008 and a PBO regional North-America fixed frame (Stable North American Reference Frame Version 1.0). The combined and individual AC products are made available in SINEX format, loosely constrained and aligned to the PBO reference frame.

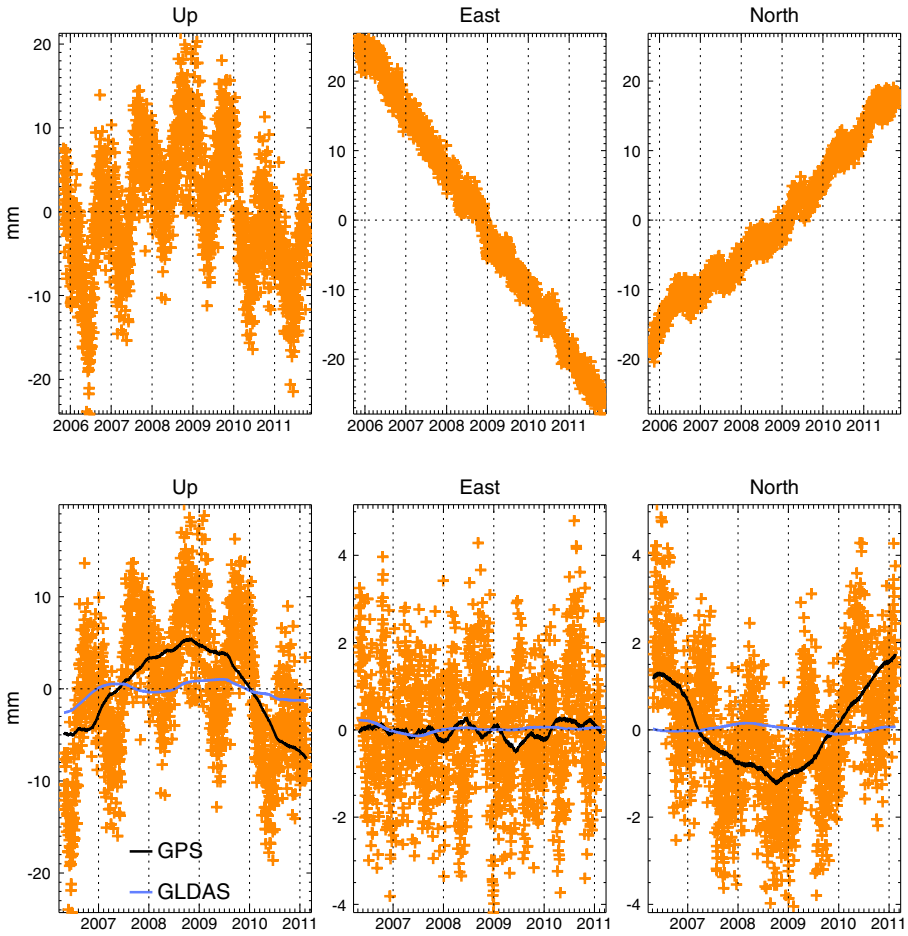

Figure 4. Daily values of the vertical (positive upward), eastward, and northward components of position, as measured at GPS site P349, located ~2 km due south of Lake Shasta. The top row shows the data as provided by the Plate Boundary Observatory Analysis Centers. The large secular trends in the horizontal components are due to a combination of tectonic motion and, to a lesser extent, reference frame drift, and are unrelated to surface loading. The orange data shown in the bottom row are obtained by fitting and removing a trend from the corresponding data shown in the top row. In the bottom row, the black curves are smoothed versions of the raw, daily, detrended data (the orange points), and the blue curves are similarly smoothed versions of the expected loading contributions from water storage outside of the lake, computed using global gridded water storage fields output from the GLDAS/Noah land surface model [*Rodell et al.*, 2004] to load an elastic Earth.

[19] Both horizontal components show dramatic secular trends, in excess of 10 mm/yr, due mostly to tectonic motion. Reference frame drift effects at this location are on the order of 0.4 mm/yr [*Altamimi et al.*, 2012; *Wu et al.*, 2012] and will also contribute to the secular trend. These signals illustrate a limitation of using horizontals to learn about loading. Namely, large trends are likely to be present in horizontals at virtually every GPS site, and they make it difficult to use the horizontals to search for purely secular trends in a loading signal. This problem can be greatly reduced in many cases by using differences between nearby stations, because the effects of tectonic motions and reference frame drift tend to be similar at closely spaced locations. Taking differences between two sites tends to amplify the contributions to the horizontal signals caused by loading between the sites, although it tends to diminish the contributions from loading occurring on the same side of both sites. It diminishes the vertical loading signal, no matter where the load is.

[20] Here, though, we look at each of the four sites individually. In this case, the presence of the large secular terms means that we are not able to use the horizontals to determine purely secular trends in the loading signal. Instead, we focus on determining the temporal 2007–2010 lake level change evident in Figure 3. The effects of that change stand out clearly in the vertical component shown in Figure 4, as a notable 2007–2009 uplift and subsequent 2009–2010 subsidence. To focus on that feature, we fit and remove a trend from each component over the entire 6 year time span and show the resulting residuals in the panels along the bottom row of Figure 4, both before and after smoothing the data with a 1 year half-width moving window to remove seasonal and other short-period terms. A 2007–2010 bump and its inverse are present in the vertical and northward components, respectively. Because the lake is almost due north of the site, the fact that the motion is upward and to the south during the first part of this event, reversing to be downward

and to the north during the second part, suggests that the lake level dropped during the first part, and rose again during the second part—which is consistent with Figure 3.

[21] It is possible that some of the GPS signal could be due to loading from changes in the distribution of water stored in the ground in the surrounding region, outside the lake. To remove those contributions, we use global, monthly, gridded estimates of total water storage changes predicted by the GLDAS/Noah land surface model [*Rodell et al*., 2004] and convolve them with *Jentzsch's* [1997] loading Green's functions for PREM, to obtain crustal motion estimates at P349. GLDAS/Noah includes contributions from snow and soil moisture, but does not include either surface water or groundwater, and so does not include contributions from Lake Shasta. The smoothed results are shown by the blue lines in the bottom row of Figure 4. The GLDAS/Noah results show a feature with a shape similar to the bump in the GPS verticals, but with a much smaller amplitude. The first row of Figure 5 shows the GPS results at P349 after removing the GLDAS/Noah predictions. The horizontal components have been rotated so that one panel shows the motion toward the lake and the other shows the motion perpendicular to that direction. The angle of the rotation is inferred from the expected direction of the horizontal displacement at P349 due to a uniform lake level rise, as shown by the arrows in Figure 2a. The top left panel of Figure 5 shows both the vertical component and the amplitude of the horizontal displacement scaled by a factor of 4.0, which is the vertical-to-horizontal amplitude expected at P349 for a uniform rise in lake level (Figure 2b). Note that the displacement is initially away from the lake, and then later reverses to be toward the lake, with relatively little motion perpendicular to the GPS-lake line during this entire period. Note also that the scaled horizontals are in good agreement with the verticals. Both these facts are consistent with the hypothesis that the P349 bump between 2007 and 2010 was caused by a change in the level of Lake Shasta.

[22] The second to fourth rows of Figure 5 are similar to the first row, but for the other three GPS sites. The results from each of those sites show a similar bump during 2007–2010. In each case, the horizontal displacements tend initially to be away from, and then later toward, the lake,

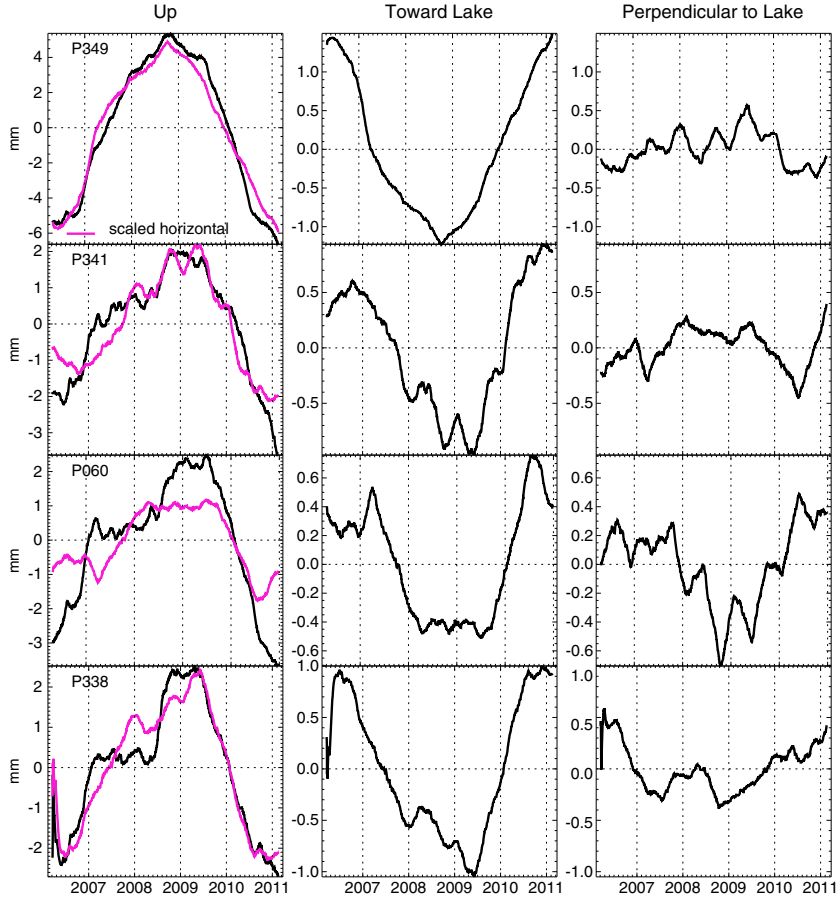

Figure 5. The detrended and smoothed vertical (upward is positive) and horizontal components of the GPS-minus-(GLDAS-induced displacement) results for the four GPS sites near Lake Shasta. Each station's horizontal components have been rotated so that the middle column shows the displacement toward the lake, and the right column shows the displacement at right angles to the direction to the lake. The purple curves in the left column show the results of scaling the amplitude of the horizontal displacements by the expected vertical-to-horizontal scaling factor for that station. The first row shows results for P349, the GPS station closest to the lake.

and the scaled horizontals (using the expected vertical-to-horizontal scale factor for that site) are in reasonable agreement with the verticals. Thus, the 2007–2010 features at each site are reasonably consistent with the hypothesis that those features are largely caused by the Lake Shasta lake level change. The consistency is not as good for these sites as it is for P349, however. That is not surprising, given that P349 is so much closer to Lake Shasta than the other sites. In fact, each of the other sites is closer to another lake (Whiskeytown Lake, located only 2–3 km from P341, and Trinity Lake, located ~15 and ~20 km from P338 and P060, respectively) than to Lake Shasta, and so could be affected by changes in those lakes as well.

[23] Suppose we assume that each site is affected only by Lake Shasta. The left column of Figure 5 shows the verticals for each of the four sites. The 2007–2010 bump is apparent at each site, but is by far the largest at P349: the site closest to the lake. If we convert each vertical time series into an equivalent Lake Shasta lake level height, using the expected lake-induced vertical displacements shown in Figure 2a, we obtain the estimates of Lake Shasta lake level height shown in Figure 6. The results inferred from the nearby station, P349, are in excellent agreement with the observed lake level observations. In fact, of the other three sites, only P338 is in notable disagreement. And even in that case, the general shape of the inferred lake level change is correct; it is the amplitude that is in error.

[24] The usefulness of the horizontals in this case is that their contributions to Figure 5—both through the horizontal direction and through the comparison between the verticals and the scaled horizontals—provide a measure of confidence as to whether we are justified in assuming Lake Shasta dominates the signal. In this example, Figure 5 suggests that Lake Shasta is likely to dominate the 2007–2010 signal at P349, but is likely to be relatively less important at the other three sites. And this, in fact, is borne out by the results shown in Figure 6.

5. Application to Glaciers in Southeast Greenland

[25] In this section we consider crustal motion measurements from the GPS site KULU (65.9753°N, 37.1149°W; see Figure 7), at Kulusuk in southeast Greenland, established in July 1996, where the largest loading signals are likely to come from dynamic changes in the flow rates and associated ice loss of nearby glaciers. There are two well-studied glaciers in this region that each drain vast regions of the ice sheet's interior: Helheim Glacier, with its mouth located about 100 km NNW of KULU, and Kangerdlugssuaq Glacier, with its mouth about 390 km NNE of KULU. In addition, there are several large glaciers with notably smaller drainage basins, lying to the NE and WSW. One of the most prominent of these is Midgaard Glacier, about 97 km NNE of KULU. Midgaard Glacier drains a far smaller region than Helheim and Kangerdlugssuaq glaciers, but its glacial area is comparable to the glacial areas of those other two glaciers. The locations of these three glaciers are shown in Figure 7.

[26] Observations of various types have shown that Helheim and Kangerdlugssuaq glaciers sped up dramatically in mid-2003, maintaining those speeds for a couple years before slowing down again in 2005–2006 [*Howat et al.*, 2007; *Murray et al.*, 2010; *Bevan et al.*, 2012]. There are indications that Helheim, at least, began accelerating again in 2009–2010 [*Moon et al.*, 2012]. There has been less attention paid to other glaciers in the region, although Midgaard Glacier has been observed to have thinned near its terminus over the last decade [*Walsh et al.*, 2012]. *Khan et al.* [2007]

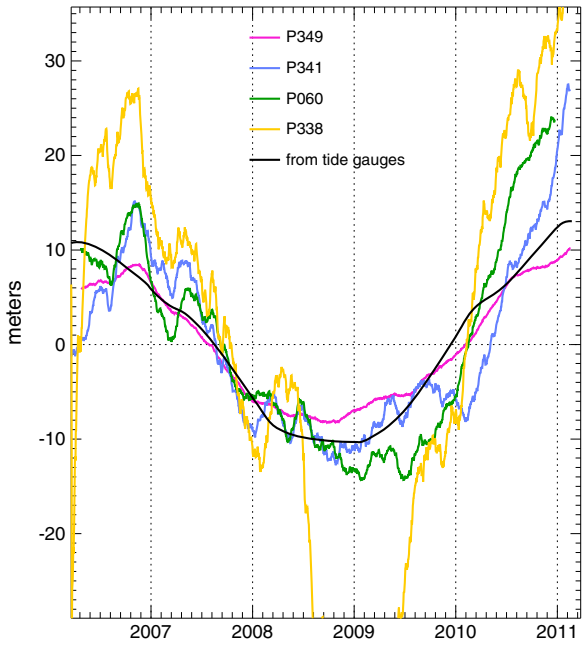

Figure 6. Lake Shasta lake levels inferred from the vertical displacements at each of the four GPS sites, as well as the lake level determined from tide gauge data.

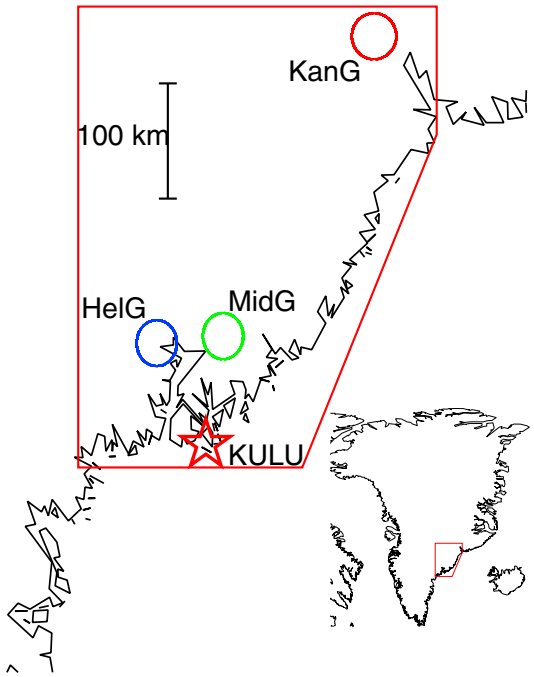

Figure 7. The southeast Greenland region in the vicinity of the GPS station KULU. The circles mark the approximate locations of the Helheim, Midgaard, and Kangerdlugssuaq glaciers.

and *Jiang et al*. [2010] noted a dramatic increase in the GPS uplift rate at KULU beginning in mid-2003, which they identified as being primarily related to ice mass loss caused by the accelerated flow of Helheim Glacier. Here, we examine whether the GPS horizontals from KULU can provide additional information about the evolving glacial mass loss in the vicinity of KULU.

[27] The GPS antenna at KULU was replaced on 10 May 1999, after an 8 month outage. Instead of trying to fit an offset across this long time window, we elect to begin our GPS analysis at the time of the antenna change. The top row of Figure 8 shows daily upward, eastward, and northward GPS components at KULU between 10 May 1999 and 31 August 2011, computed using the 6.1.2 GIPSY-OASIS software package [*Zumberge et al*., 1997] released in January 2012 and developed at the Jet Propulsion Laboratory (JPL). We use GPS orbits, Earth orientation, and clock products provided by JPL and based on a global network of GPS sites. All GPS data are processed in the same manner as described by *Wahr et al*. [2001], except that solutions are aligned with the ITRF08 reference frame through the standard application of translation, rotation, and scale factors [*Altamimi et al*., 2011].

[28] Both horizontal components show secular trends in excess of 15 mm/yr, due mostly to a combination of tectonic motion, reference frame drift (on the order of 0.4 mm/yr at this location), and viscoelastic glacial isostatic adjustment, that prohibits us from using the horizontals to study purely secular changes in loading. Instead, we use the fact noted above that the rate of nearby glacial ice loss apparently increased in 2003, and we focus on determining the spatial and temporal distribution of mass loss relative to the pre-2003 trend. The effects of the 2003 increase stand out clearly in the vertical component as a notable upward swing at about this time [*Khan et al*., 2007; *Jiang et al*., 2010]. Accordingly, we fit a trend to each GPS component using data only through the end of 2002 and subtract those trends from the entire 1999.3–2011.7 time series. This should

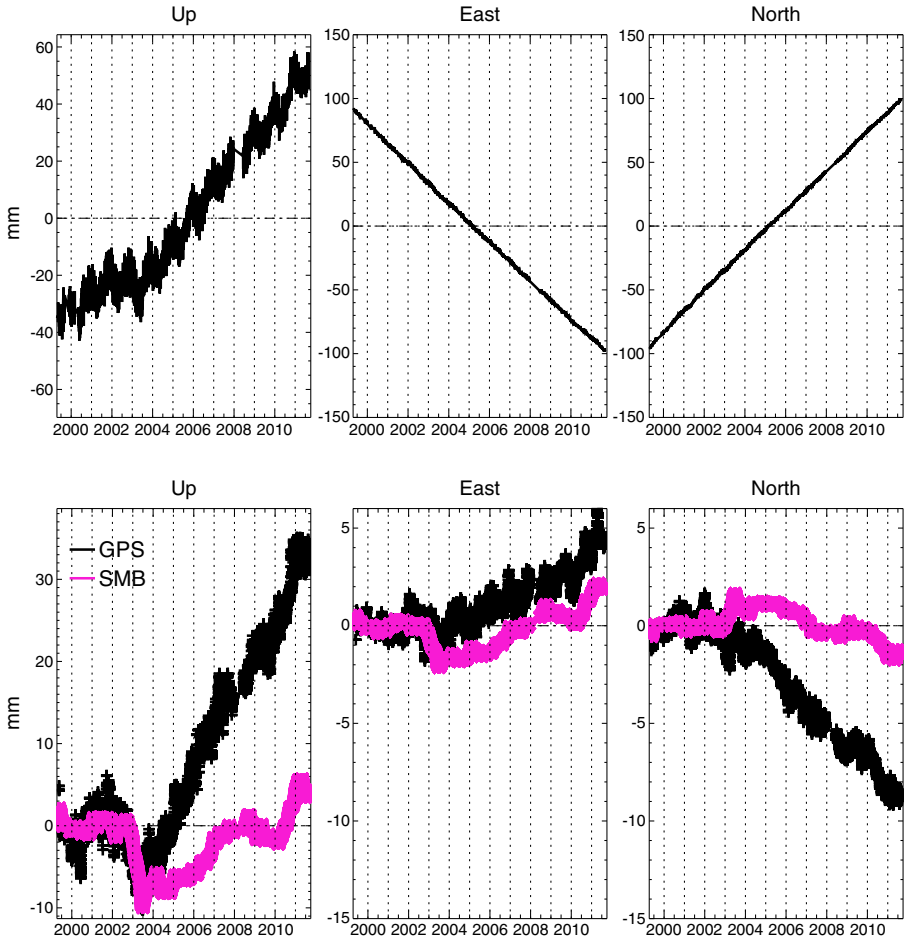

Figure 8. Top row: daily values of the vertical (positive upward), eastward, and northward components of position, as determined from GPS data at KULU between 10 May 1999 (the date of the most recent KULU antenna change) and 31 August 2011. The large secular trends in the horizontal components are due to a combination of tectonic motion and, to a lesser extent, reference frame drift, and are unrelated to surface loading. Bottom row: the data shown in black are obtained by fitting a trend to the pre-2003.0 data, and removing that trend, as well as seasonal terms, from the corresponding data shown in the top row. The purple values are similarly detrended and smoothed versions of the expected loading contributions from surface mass balance (SMB), computed using gridded SMB values from *van den Broeke et al*. [2009] and *Van Angelen et al*. [2012] to load an elastic Earth.

remove contributions from tectonic motion and from the Earth's viscoelastic response to ice variations in the near and distant past, since both those contributions are almost certain to appear as linear trends over the entire 1999.3–2011.7 time span. There are no sizable earthquakes or other sources of episodic tectonic motion in this region; and the viscoelastic decay times for a cratonic setting like Greenland are long enough that viscoelastic deformation rates caused by past ice variability would be nearly constant at decadal and longer time scales [e.g., *Wahr and Han*, 1998].

[29] The results are shown in black in the bottom row of Figure 8, after also removing seasonal terms and smoothing the residuals with an 11 day moving window. All three components show clear changes in slope in 2003. Our focus below is on the mass variations responsible for these and subsequent changes in slope. The eastward and northward components indicate post-2003.0 motion to the SSE, which is indicative of either a net mass loss NNW of KULU, or a net mass gain SSE of KULU. The fact that the vertical shows post-2003.0 uplift implies there was a net mass loss. The implication from the horizontals is then that this mass loss occurred NNW of KULU, which is in the general direction of Helheim Glacier.

[30] To isolate the contributions from dynamic changes of nearby glaciers, we remove the predicted loading signal caused by Greenland surface mass balance (SMB), using monthly, gridded SMB estimates from the regional atmospheric climate model RACMO2 [*van den Broeke et al*., 2009; *Van Angelen et al*., 2012]. The SMB results represent the effects of snowfall, sublimation, and surface melting (taking into account possible subsequent refreezing). As such, they include all loading contributions from the Greenland ice sheet except those due to mass redistribution caused by the horizontal flow of ice. Those dynamic flow effects, particularly the mass loss due to changes in glacier discharge rates into the ocean, are the focus of this application. Since glacier mass loss is spatially much more concentrated than SMB loading, it is better suited to the analysis approach outlined above.

[31] The bottom row of Figure 8 shows, in purple, the loading effects caused by convolving the gridded SMB model output with loading displacement Green's functions for Earth model PREM (with a continental crust), as tabulated by *Jentzsch* [1997]. A trend has been fit to (and removed from) the SMB results using the same pre-2003.0 time span used to fit to the GPS data; seasonal terms have been removed as well. Note that the SMB results show changes in the trend at about the same time as the GPS data (i.e., in mid-2003), in a direction that suggests post-2003.0 SMB mass loss to the west of KULU (i.e., there is a dominant eastward shift in the trend). The gridded SMB fields do, in fact, show a notable trend in mass loss west of KULU that began in 2003. The SMB amplitudes are notably smaller than those from GPS, except in the eastward component where they are comparable.

[32] We subtract the SMB displacement estimates from the GPS residuals and interpret the remainder as due to loading caused by dynamic effects of nearby glaciers. To determine the average direction of the GPS-minus-SMB horizontals, we fit a direction angle to the detrended horizontals over the post-2003.0 data. We obtain a direction of motion that's oriented 21° counterclockwise from south. We thus deduce that, on average, either (a) there was mass gain centered along a line oriented 21° counterclockwise from south, or (b) there was mass loss centered along a line oriented in the opposite direction: i.e., 21° counterclockwise from north. The vertical motion is upward. Thus there must have been net mass loss during this time period, implying that case b is preferred.

[33] Figure 9a shows that the line oriented 21° counterclockwise from north passes along the eastern edge of Helheim Glacier, between the centers of Helheim and Midgaard glaciers. Since the argument above implies the post-2003.0 mass loss was centered on average along that line, it is natural to conclude that the source of the post-2003.0 KULU GPS signal is likely to have been dominated by mass changes from Helheim, but possibly with contributions from Midgaard as well. Because Kangerdlugssuaq Glacier is so much farther from KULU, its contributions are unlikely to have been important.

[34] Figures 9b–9d show (in blue) the GPS displacement components after the SMB loading and pre-2003.0 trends have been removed. The horizontals in Figures 9c and 9d have been rotated into components along and perpendicular to the best-fitting direction of motion (21° counterclockwise from south). A positive value of the perpendicular component implies a displacement toward the westward side of that direction (i.e., toward 69° clockwise from south.) The most obvious features in Figures 9b–9d are the abrupt shifts in slope that begin in mid-2003 in Figures 9b and 9c that suggest, even more clearly, that there was a sudden increase in the rate of nearby mass loss and that it was centered along the purple line in Figure 9a.

[35] Figure 9b also shows (in orange) the amplitude of the horizontal displacement multiplied by 2.2. The theoretical arguments above show that for a single concentrated load, a factor of 2.2 is appropriate for the vertical-to-horizontal ratio over a wide range of distances to that load. Figure 9b shows that prior to 2006, the scaled horizontals agree reasonably well with the verticals. But starting in 2006, the scaled horizontals begin to be increasingly smaller than the verticals. This suggests that prior to 2006, a single concentrated load was likely to have dominated the GPS signal, but that starting in 2006 other loads may have become relatively important.

[36] Figure 9d shows that the displacements perpendicular to the purple line in Figure 9a are more-or-less flat, which suggests that the spatial distribution of the mass change stayed reasonably constant over the entire 1999.3–2011.7 time span. There are, however, suggestions of some non-negligible interannual variations. For example, there is a downward curvature to the Figure 9d results starting in mid-2003, suggesting that the direction of motion began heading slightly eastward of the average direction at about that time. This suggests the sudden mid-2003 increase in mass loss rate was concentrated slightly to the west of the purple line in Figure 9a, i.e., more over the center of Helheim Glacier. The Figure 9d results then start to bend upward in 2004, indicating that the direction of motion was starting to head more westerly—consistent with a mass loss rate that was concentrated more to the east of Helheim. Figure 9b also suggests there might have been a slight decrease in the rate of upward motion at the end of 2005 that lasted for 2–3 years, implying a corresponding decrease in the total mass loss rate in the vicinity of KULU.

[37] Taken together, these results are consistent with the following qualitative picture. The post-2003.0 change in

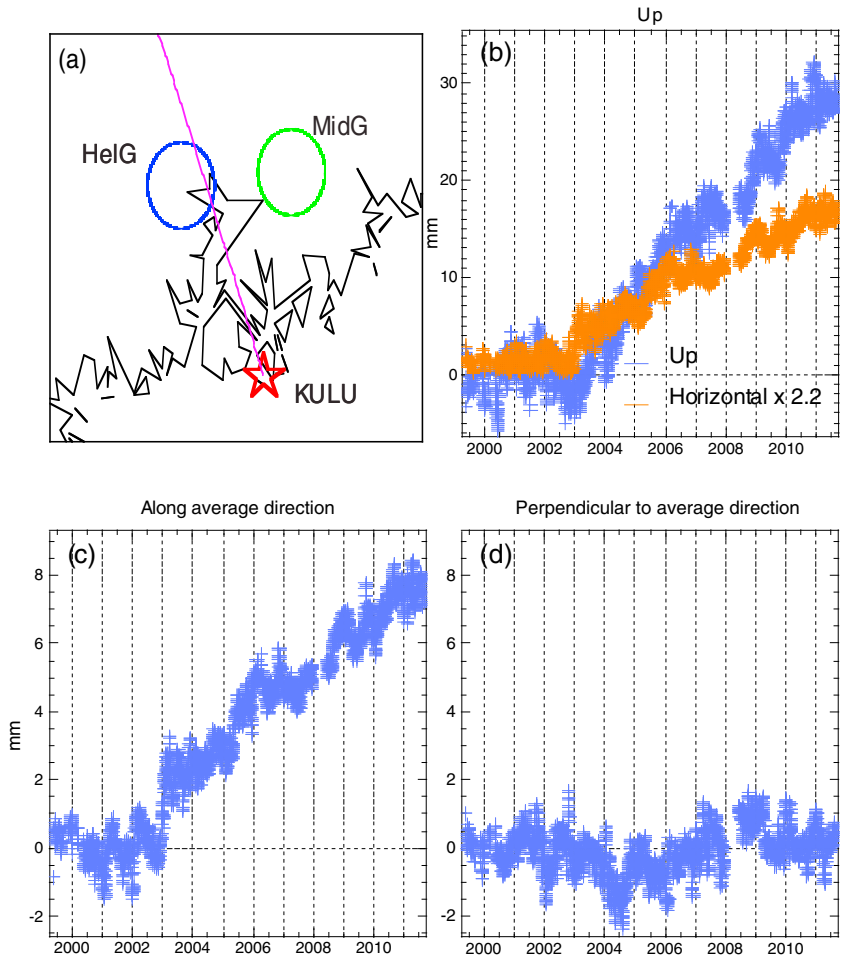

Figure 9. (a) The average direction of horizontal motion at KULU after 2003.0, and relative to the 1999.3–2003.0 trend, is in the opposite direction of the purple line. This implies that the average direction to the mass loss causing that motion, is somewhere along the purple line. (b–d) The vertical (up is positive) and horizontal components of the GPS-minus-(SMB-induced displacement) results, after removing the 1999.3–2003.0 trend and seasonal terms. The horizontal displacements have been rotated so that Figure 9c shows the displacement along the average direction (21° counterclockwise from south; so SSE), and Figure 9d shows the displacement at right angles to that direction (positive is toward the westward side of the average direction). The orange results in Figure 9b are computed by multiplying the amplitude of the horizontal displacement by a vertical-to-horizontal ratio of 2.2.

mass loss, as it affected KULU, consisted of a dominant loss from Helheim glacier. In 2005–2006, the Helheim mass loss rate decreased, and mass loss rates from farther east, e.g., from Midgaard Glacier, became relatively more important. The decreased mass loss from Helheim caused a decrease in the total uplift rate, and swung the direction of the horizontals around clockwise, so that it pointed away from locations lying farther east of Helheim. Figures 9b–9d suggest that the 2005–2006 changes reversed in ~2009, when the Figure 9d trend flattened out again and the uplift rate (Figure 9b) increased. This suggests that Helheim might have sped up again at about that time.

[38] To quantify these ideas, we assume the total nearby glacial mass loss is concentrated in Helheim and Midgaard glaciers. Let λ_1 and λ_2 be the angles, counterclockwise from north, describing the directions to Helheim and Midgaard glaciers, respectively. Let u_1 and v_1 be the upward and horizontal displacements caused by the removal of a load at Helheim, and u_2 and v_2 be the displacements caused by the removal of a load at Midgaard. Then the total upward, northward, and eastward components of displacement are (noting that a mass loss causes horizontal motion away from the mass):

$$u_{\text{tot}} = u_1 + u_2 \tag{6}$$

$$v^N_{\text{tot}} = -v_1 \cos\lambda_1 - v_2 \cos\lambda_2 \tag{7}$$

$$v^E_{\text{tot}} = v_1 \sin\lambda_1 + v_2 \sin\lambda_2 \tag{8}$$

[39] Suppose we assume vertical-to-horizontal ratios of D_1 and D_2 for the two glaciers. Then (6) becomes:

$$u_{\text{tot}} = v_1 D_1 + v_2 D_2 \tag{9}$$

[40] We assume $D_1 = D_2 = 2.2$, since the nearest margins of the two glaciers are on the order of 100 km from KULU, and

Figure 1c shows that at this distance $D = 2.2$ is a reasonable assumption for a wide range of glacier sizes. We use (7)–(9) to fit v_1 and v_2 to the smoothed and detrended GPS-minus-SMB data shown in Figures 9b–9d, at every time.

[41] Our results for v_1 and v_2, shown in Figure 10, are our estimates of the contributions of Helheim and Midgaard glaciers, respectively, to horizontal motion at KULU. Because we have already removed the pre-2003.0 trend from all GPS and SMB components, the Figure 10 results indicate the glacial contributions relative to their pre-2003 trend values. Thus, to obtain the total horizontal signal from each glacier, the Figure 10 results would have to be added to whatever trend each glacier was contributing prior to 2003.

[42] The Figure 10 results show an overall upward trend for the contributions from both Helheim and Midgaard. This suggests that both these glaciers were losing mass after 2003.0 at a greater rate than their 1999.3–2003.0 average. Helheim's initial upward trend appears to have begun a year earlier than Midgaard's (mid-2003 versus mid-2004). The steeper slope in the Helheim data indicates that up until the end of 2005, the contributions from Helheim were increasing more rapidly than those from Midgaard. But in 2006, the Helheim contributions slowed down, whereas the Midgaard contributions continued at about their same rate. Note that because the pre-2003 trends have been removed, this does not necessarily mean that the Helheim loading signal was holding steady. Instead, it only means that the mass loss rate was about equal to its pre-2003 level. Figure 10 also shows that starting sometime in 2009 the contributions from Helheim increased again, though they may have stabilized near the end of 2010. Midgaard's contributions (relative to its 1999.3–2003.0 trend) seem to have flattened out in late 2008, and to have held steady thereafter. These general conclusions about the temporal evolution of Helheim's behavior (i.e., speed-up in 2003, slowdown in 2005, speed-up again in 2009) are consistent with published results based on various satellite data types [see, e.g., *Howat et al.*, 2007; *Stearns and Hamilton*, 2007; *Murray et al.*, 2010; *Moon et al.*, 2012; *Bevan et al.*, 2012]. In contrast, few comparable published satellite results for Midgaard Glacier exist. Recently *Walsh et al.* [2012] studied 37 glaciers in southeast Greenland and reported that the largest retreat occurred at Midgaard glacier, which retreated 9.2 km during 2000–2010, most of which occurred during 2005–2010 (see their Figure 6). At a distance of 15 km upstream, Midgaard thinned by more than 50 m during this period. This thinning of Midgaard glacier is comparable with the observed thinning of Helheim and Kangerdlugssuaq glaciers.

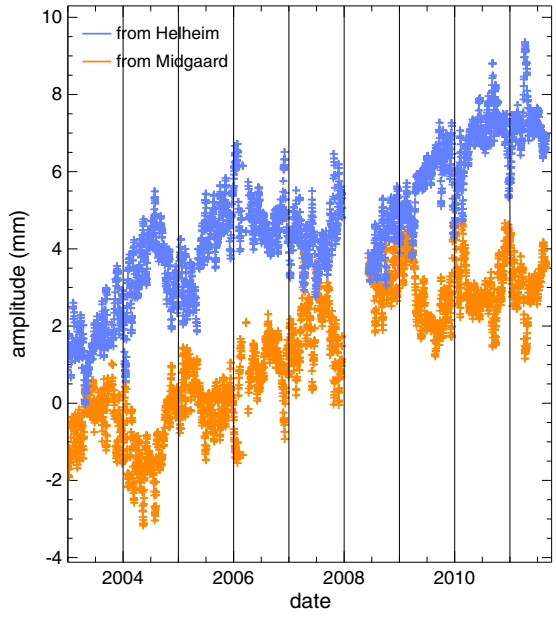

Figure 10. Solutions for the contributions to KULU's horizontal signals, relative to the 1999.3–2003.0 trend, from Helheim and Midgaard glaciers.

6. Discussion and Conclusions

[43] Although GPS observations of crustal deformation have frequently been used to study surface loading, the focus of those studies has usually been on the vertical component. Horizontal displacements have not received the same level of attention, for at least two reasons. One is that loading-induced horizontal displacements tend to be much smaller than vertical displacements. As described above, the vertical-to-horizontal ratio is 2-to-3 for a concentrated load and can be much larger than that for the more usual case where the load is spread over a wide region. There is less noise in GPS horizontals than in the verticals [*Ray et al.*, 2011]. Still, horizontal loading signals can be difficult to identify. The second reason is that large trends are usually present in horizontal components, due primarily to tectonic motion with an additional small contribution from reference frame drift. Those trends, though, are an issue for loading studies only if the goal is to identify secular changes. And, even then, their impact can presumably be reduced by analyzing differences between data from nearby stations, if available, rather than focusing on single-station data.

[44] In this paper, we have described a few simple concepts that can be used to incorporate horizontals into loading studies. We showed how those concepts can be implemented by applying them to two specific cases: an analysis of data from northern California to infer changes in the level of Lake Shasta, and the analysis of data from a single site (KULU) in southeast Greenland to monitor mass changes in nearby glaciers.

[45] The Lake Shasta study was included solely for illustrative purposes. There is little direct value in our GPS-derived Lake Shasta lake levels, since tide gauge estimates already exist and, in fact, were used above to verify our GPS results. The analysis does, however, show how horizontal components can be used to augment vertical measurements in loading studies in general and, specifically, how GPS results could be useful for monitor levels of a nearby lake or reservoir in the absence of tide gauge information.

[46] The Greenland study was also included partly as an example of how horizontal measurements can be used to augment vertical observations to improve and extend a loading analysis. But in this case the results are of value in their own right. By using all three components, we were able to infer temporal patterns of multi-year mass loss from Helheim and Midgaard glaciers. We concluded that (a) both glaciers experienced dramatic increases in their mass loss rates in 2003–2004 (Helheim in 2003, Midgaard in 2004), (b) Helheim's mass loss rate decreased in late 2005, but

Midgaard's did not, and (c) Helheim's mass loss rate increased again in 2008–2009 before leveling off in late 2010, whereas Midgaard's rate was roughly equal to its 1999.3–2003.0 rate from late 2008 until the end of the time series (late 2011). We are not able to actually determine numbers for the mass loss rates, because the glacial catchments are spread over large regions (particularly for Helheim), and the KULU crustal motion is not equally sensitive to all points within those catchments. Basically, the GPS estimates provide a weighted average of the mass loss across a catchment, where the weighting is determined by the load Green's function and is not uniform across the catchment, whereas an estimate of the total mass loss is a catchment average with a uniform weighting.

[47] Our interpretation is not without ambiguity. For example, it seems indisputable that Helheim glacier would be a dominant contributor to the KULU loading signal. And the GPS measurements do imply there had to have been contributions from at least one other location. But, although our assumptions that there was a single additional glacier rather than multiple sources and that Midgaard Glacier was that single glacier seem reasonable, they are still both somewhat arbitrary. The limitation in this case is that we are working with data from only a single GPS site. The GNET (GPS Network in Greenland) network, consisting of over 50 permanent GPS sites installed along the Greenland ice margin during 2007–2009, vastly improves the ability to monitor ice loss with GPS [*Bevis et al*., 2012]. As GNET data continue to be acquired, it should become possible to use horizontal components from more than one station to triangulate on glacier locations, and to remove much of the ambiguity that is unavoidably present when using data from just one site.

[48] **Acknowledgments.** We thank Jeannie Sauber-Rosenberg and Freysteinn Sigmundsson for helpful reviews. J. Wahr was partially supported by NASA grant NNX06AH37G and by JPL contract 1390432. S. A. Khan was supported by The Danish Council for Independent Research-Natural Sciences (FNU). L. Liu was partly supported by NASA Earth and Space Science Fellowship Program-NNX08AU85H and George Thompson Postdoctoral Fellowship, Stanford University. J. H. van Angelen and M. R. van den Broeke were supported by Utrecht University and the Polar Program of the Netherlands Organization for Scientific Research (NWO/ALW). Processed GPS products used for this study are produced by Plate Boundary Observatory Analysis Centers, funded by UNAVCO for EarthScope and supported by the National Science Foundation, at Central Washington University, the New Mexico Institute of Mining and Technology, and the Analysis Center Coordinator at the Massachusetts Institute of Technology.

References

Altamimi, Z., X. Collilieux, and L. Métivier (2011), ITRF2008: An improved solution of the international terrestrial reference frame, *J. Geod.*, *85*(8), doi:10.1007/s00190-011-0444-4.

Altamimi, Z., L. Métivier, and X. Collilieux (2012), ITRF2008 plate motion model, *J. Geophys. Res.*, *117*, B07402, doi:10.1029/2011JB008930.

Bevan, S. L., A. J. Luckman, and T. Murray (2012), Glacier dynamics over the last quarter of a century at Helheim, Kangerdlugssuaq and 14 other major Greenland outlet glaciers, *The Cryosphere Discuss*, *6*, 1637–1672, www.the-cryosphere-discuss.net/6/1637/2012/, doi:10.5194/tcd-6-1637-2012.

Bevis, M., D. Alsdorf, E. Kendrick, L. P. Fortes, B. Forsberg, R. Smalley Jr., and J. Becker (2005), Seasonal fluctuations in the mass of the Amazon River system and Earth's elastic response, *Geophys. Res. Lett.*, *32*, L16308, doi:10.1029/2005GL023491.

Bevis, M., et al. (2012), Bedrock displacements in Greenland manifest ice mass variations, climate cycles and climate change, *Proc. Nat. Acad. Sci.*, doi:10.1073/pnas.1204664109.

Christian-Smith, J., M. C. Levy, and P. H. Gleick (2011), Impacts of the California Drought from 2007–2009, Report of the Pacific Institute, Oakland, CA, 103 pp.

Dahlen, F. (1976), The passive influence of the oceans upon the rotation of the earth, *Geophys. J. R. Astr. Soc.*, *46*, 363–406.

Dziewonski, A., and D. L. Anderson (1981), Preliminary reference Earth model, *Phys. Earth Planet. Inter.*, *25*, 297–356.

Farrell, W. (1972), Deformation of the Earth by surface loads, *Rev. Geophys. Space Phys.*, *10*, 761–797.

Grapenthin, R., F. Sigmundsson, H. Geirsson, T. Arnadottir, and V. Pinel (2006), Icelandic rhythmics: Annual modulation of land elevation and plate spreading by snow load, *Geophys. Res. Lett.*, *33*, L24305, doi:10.1029/2006GL028081.

Heki, K. (2004), Dense GPS array as a new sensor of seasonal changes of surface loads, in The State of the Planet: Frontiers and Challenges in Geophysics, Geophys. Monogr. Ser., vol. 150, edited by R. S. J. Sparks, and C. J. Hawkesworth, pp. 177–196, AGU, Washington, D. C., doi:10.1029/150GM15.

Howat, I. M., I. R. Joughin, and T. A. Scambos (2007), Rapid changes in ice discharge from Greenland outlet glaciers, *Science*, *315*, 1559–1561.

Jentzsch, G. (1997), Earth tides and ocean tidal loading. in Tidal Phenomena, edited by H. Wilhelm, W. Zurn, and H. G. Wenzel, pp. 145–171, Springer-Verlag, Berlin.

Jiang, Y., T. H. Dixon, and S. Wdowinski (2010), Accelerating uplift in the North Atlantic region as an indicator of ice loss, *Nat. Geosci.*, *3*, 404–407, doi:10.1038/ngeo845.

Khan, S. A., J. Wahr, L. A. Stearns, G. S. Hamilton, T. van Dam, K. M. Larson, and O. Francis (2007), Elastic uplift in southeast Greenland due to rapid ice mass loss, *Geophys. Res. Lett.*, *34*, L21701, doi:10.1029/2007GL031468.

Moon, T., I. Joughin, B. Smith, and I. Howat (2012), 21st-century evolution of Greenland outlet glacier velocities, *Science*, *336*, 576–578.

Murray, T., et al. (2010), Ocean regulation hypothesis for glacier dynamics in Southeast Greenland and implications for ice sheet mass changes, *J. Geophys. Res.*, *115*, F03026, doi:10.1029/2009JF001522.

Pinel, V., F. Sigmundsson, E. Sturkell, H. Geirsson, P. Einarsson, M. T. Gudmundsson, and T. Hognadotir (2007), Discriminating volcano deformation due to magma movements and variable surface loads: Application to Katla subglacial volcano, Iceland, *Geophys. J. Int.*, *169*(1), 325–338, doi:10.1111/j.1365-246X.2006.03267.x.

Ray, J., X. Collilieux, P. Rebischung, T. van Dam, and Z. Altamimi (2011), Consistency of crustal loading signals derived from models and GPS: Inferences for GPS positioning errors, Invited Presentation, American Geophysical Union, Fall 2011, San Francisco, California.

Rodell, M., et al. (2004), The global land data assimilation system, *Bull. Am. Meteorol. Soc.*, *85*(3), 381–394, doi:10.1175/BAMS-1185-1173-1381.

Sauber, J., G. Plafker, B. F. Molnia, and M. A. Bryant (2000), Crustal deformation associated with glacial fluctuations in the eastern Chugach Mountains, Alaska, *J. Geophys. Res. Solid Earth*, *105*(B4), 8055–8077, doi:10.1029/1999JB900433.

Sauber, J. M., and B. F. Molina (2004), Glacier ice mass fluctuations and fault instability in tectonically active Southern Alaska, *Global Planet. Change*, *42*(1-4), 279–293, doi:10.1016/j.gloplacha.2003.11.012.

Stearns, L. A., and G. S. Hamilton (2007), Rapid volume loss from East Greenland outlet glaciers quantified using repeat stereo satellite imagery, *Geophys. Res. Lett.*, *34*, L05503, doi:10.1029/2006GL028982.

Van Angelen, J. H., J. T. M. Lenaerts, S. Lhermitte, X. Fettweis, P. Kuipers Munneke, M. R. van den Broeke, E. van Meijgaard, and W. G. Greuell (2012), Sensitivity of Greenland ice sheet surface mass balance to surface albedo parameterization: A study with a regional climate model, *The Cryosphere*, *6*(5), 1175–1186, doi:10.5194/tc-6-1175-2012.

van Dam, T., J. Wahr, and D. Lavallée (2007), A comparison of annual vertical crustal displacements from GPS and Gravity Recovery and Climate Experiment (GRACE) over Europe, *J. Geophys. Res.*, *112*, B03404, doi:10.1029/2006JB004335.

Van den Broeke, M. R., J. Bamber, J. Ettema, E. Rignot, E. Schrama, W. J. van de Berg, E. van Meijgaard, I. Velicogna and B. Wouters (2009), Partitioning recent Greenland mass loss, *Science*, *326*, 984–986.

Wahr, J., and D. Han (1998), Geodetic techniques for estimating changes in polar ice, in Dynamics of the Ice Age Earth; A Modern Perspective, edited by P. Wu, pp. 497–508, Trans Tech Publications Ltd., Switzerland.

Wahr, J., T. van Dam, K. Larson, and O. Francis (2001), Geodetic measurements in Greenland and their implications, *J. Geophys. Res.*, *106*, 16,567–16,582.

Walsh, K. M., I. M. Howat, Y. Ahn, and E. M. Enderlin (2012), Changes in the marine-terminating glaciers of central east Greenland, 2000–2010, *The Cryosphere*, *6*, 211–220, 2012, doi:10.5194/tc-6-211-2012.

Wu, X., J. Ray, and T. van Dam (2012), Geocenter motion and its geodetic and geophysical implications, *J. Geodyn.*, *58*, 44–61, doi:10.1016/j.jog.2012.01.007.

Zumberge, J. F., M. B. Heflin, D. C. Jefferson, M. M. Watkins, and F. H. Webb (1997), Precise point positioning for the efficient and robust analysis of GPS data from large networks, *J. Geophys. Res.*, *102*, 5005–5017.